In-Situ SEM and EBSD Analysis on Plastic Behavior of Laser Beam Welding Ti-6Al-4V Alloy

DANG Ning[1, 2], LIU Lingyu[3], LAVOGIEZ Cyril[2], MAIRE Eric[2], MA Chaoli[1], ZHOU Lian[1, 4]

(1. School of Materials Science and Engineering, Beihang University, Beijing 100191, China)
(2. INSA de Lyon, Mateis UMR 5510, Villeurbanne 69621, France)
(3. Baoti Group Co., Ltd., Baoji 721014, China)
(4. Northwest Institute for Nonferrous Metal Research, Xi'an 710016, China)

Abstract: EBSD and *in-situ* SEM were used to study the plastic behavior of laser beam welding Ti-6Al-4V. Due to the high weld temperature (exceeding the β-transus) and high cooling rate, $\beta \rightarrow \alpha'$ martensitic transformation occurs. Within the fusion zone, only acicular morphology exists, while in 1st heat affected zone (HAZ) and 2nd HAZ, these acicular laths globalize, which show an obvious microstructural gradient. The result of the *in-situ* plastic deformation shows the deformation can be divided into 2 stages. In the first stage of the deformation, either slipping or twinning can occur. It depends on whether the initial orientation can respect <120>//TA (tensile axis) by rotating the grains or not. While in the second stage, only slipping can be found.

Key words: crystallographic orientation; *in-situ* SEM; plastic deformation; laser beam welding; Ti-6Al-4V alloy
CLC number: TG146.23 **Document code**: A **Article ID**: 1674-3962 (2019)03-0279-07

激光焊接 Ti-6Al-4V 钛合金塑性行为的原位 SEM/EBSD 分析

党 宁[1,2], 刘玲玉[3], LAVOGIEZ Cyril[2], MAIRE Eric[2], 马朝利[1], 周 廉[1,4]

(1. 北京航空航天大学材料科学与工程学院, 北京 100191)
(2. INSA de Lyon, Mateis UMR 5510, Villeurbanne 69621, France)
(3. 宝钛集团有限公司, 陕西 宝鸡 721014)
(4. 西北有色金属研究院, 陕西 西安 710016)

摘 要: 选用原位 SEM/EBSD 显微术分析研究了 Ti-6Al-4V 钛合金的焊接区域的变形行为。研究发现, 由于焊接时高的焊接温度(在 β 相变点之上)和急剧的冷却速率, 导致 $\beta \rightarrow \alpha'$ 马氏体相变的发生。SEM 观察发现, 在焊缝区只存在有针状的 α' 马氏体形貌, 而在焊接第一热影响区和第二热影响区, 针状 α' 相逐渐发生球化, 形成了明显的显微组织梯度过渡。在对焊接区域进行 SEM/EBSD 下的原位拉伸实验后发现, 该区域的塑性变形可划分为两个阶段。变形的第一阶段, 滑移变形或孪生变形均有可能发生, 这取决于晶粒的初始晶体学取向是否可通过旋转来匹配<120>//TA(拉伸方向); 而在变形的第二阶段, 只发生滑移变形。

关键词: 晶体学取向; 原位 SEM; 塑性变形; 激光焊接; Ti-6Al-4V 钛合金

1 Introduction

Titanium alloys, because of high strength, low density and excellent corrosion resistance, are increasingly becoming essential materials for aircraft fabrication, ship-building and auto car industry. Besides, Ti alloys are also widely used in the emerging biomedical prostheses applications due to the excellent biocompatibility[1,2]. Ti-6Al-4V alloy, which is also called Ti64 or TA6V, is accounting for around 50% in tonnage of total Ti alloys production[3]. Thus, this alloy has drawn many researchers' attentions to enhance its mechanical properties.

Generally, welding procedure and equipment used for other metallic materials (such as steels or Al alloys), for instance, tungsten inert gas (TIG) welding, laser beam welding (LBW), electron beam welding (EBW), friction welding *et al.*, can be carried on commercial titanium and most of Ti alloys[4-8]. Comparing with other welding technologies, LBW has the most considerable flexibility for joining titanium

Received date: 2017-06-15 Revised date: 2017-10-09
First author: Dang Ning, Male, Born in 1987, Doctoral candidate, Email: dangning@buaa.edu.cn
DOI: 10.7502/j.issn.1674-3962.2019.03.10

alloys, either autogenously or with the use of filler wire or powder[9]; Moreover, as laser welding permits the generation of a key hole that effectively concentrates the energy input into a small area, there is good potential to join titanium alloys since the variation of microstructure is confined within the weld region and a narrow heat affected zone(HAZ)[10]; therefore, titanium alloy joint welded by LBW has fine grains[11]. Besides, Zhang's work[12] revealed whether a titanium alloy joint is welded by LBW or by traditional fusion welding, the residual stress distributions in these two kinds of joints are almost the same; however, the distribution zone is much narrower when LBW was used.

Recently, plenty of researchers focused on the effects of laser welding parameters on the morphology and mechanical properties of welded joints. Gao *et al.*[13] compared the properties of Ti-6Al-4V alloy joints between pulsed Nd∶YAG laser welding and TIG. Their result shows that the welded joint by LBW has small overall residual distortion, fine microstructure, narrow HAZ, high Vickers hardness, when comparing with TIG. Cao and Jahazi[14] indicated that comparing with base metal specimens, laser welded joints of Ti-6Al-4V had slightly higher joint strength but significant weak ductility. Squillace *et al.*[15] has modified the welding rate and laser's power, their work proved Cao and Jahazi's indication. Furthermore, this work indicated that fatigue strength of the welds can be increased by partially or totally eliminating the underfill regime. Zhang *et al.*[16] revealed significant relationship between the damage evolution of continuous laser-welded joints subjected to tensile load and gradient distribution of microstructure in the welded joint.

Although we have well known the influence of processing parameters on microstructure and mechanical properties, little attention is paid on the crystallographic orientation evolution in welding zone during the plastic deformation. Thanks to the EBSD technology, we know that crystallography orientation or texture may affect the crack nucleation and growth. Hence, it is needed to analyze the role of crystallography orientation in the welding zone during the plastic deformation procedure.

Aiming at this goal, this current work was to analyze the relationship between plastic deformation behavior and crystallographic orientation evolution for the welding zone of TA6V alloy. To get better understanding of the plastic behavior of the welding zone, *in-situ* tensile tests based on SEM were carried out; then the crystallography orientation and deformation behavior were measured and evaluated by EBSD method systematically.

2 Experiment

2.1 Material and welding process

As-received specimens were annealed Ti-6Al-4V alloy sheet, which have been welded by laser homogeneously. Welding parameters were selected from Migliarini's thesis[17] and Cryil's thesis[18]. All the welding details can be found in Migliarini's thesis[17] and Cryil's thesis[18].

Each specimen was welded together from two parts of tensile sample in the approach of homogeneous laser welding process. The geometry of the specimen can be found in the Fig. 1a and the dimension is given in Fig. 1b. It is worth to mention that only the gage region was welded (as shown in Fig. 1a). A small gage length can be noticed when comparing to the dimension of the specimen.

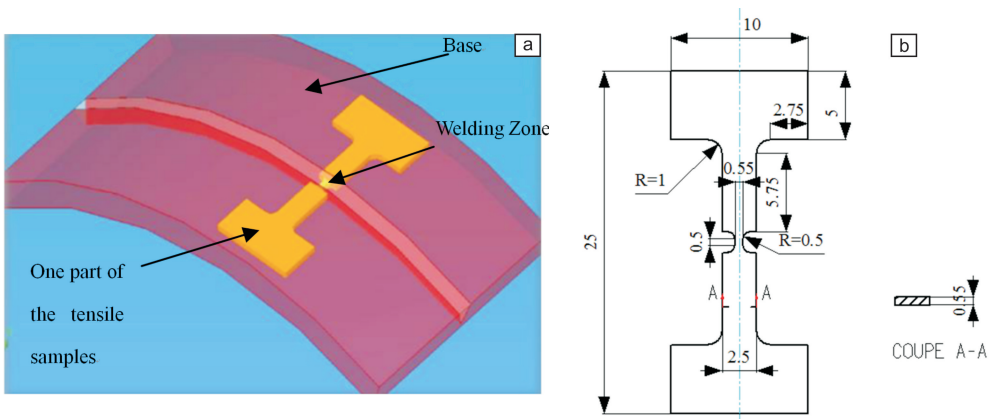

Fig. 1 Schematic figures for laser welding procedure(a) and the geometry and dimension (b) of the specimen used for *in-situ* tensile work

2.2 *In-situ* tensile test with SEM

For *in-situ* SEM and EBSD analysis, the surface of the specimen was carefully treated after removing from the base, following by metallographic preparation procedure recommended by Struers© . The first step was surface grinding by using SiC paper (up to a 2400 grid). Then, with the help of adapted apparatus, polishing work of 3 μm and 1 μm were done. For the final step, vibratory polishing was carried out for 4 h with a mixed solution of colloidal silica (OP-S) and hydrogen peroxide (H_2O_2).

In-situ tensile test was performed based on Supra 55VP (Carl Zeiss Microscopy) SEM. Standard parameters (15 ~ 20 kV, working distance of 13 mm) were used for secondary electron (SE) and backscattered electron (BSE) imaging. The *in-situ* tensile work was performed at a constant displacement rate of 0.002 mm/s. Two interruptions were performed when the deformation strain was achieved at around $\varepsilon = 10\%$ and 12% respectively. This tensile work was ended at around $\varepsilon = 14\%$ in order to avoid the influence of the severe plastic deformation on the EBSD mapping. It is worth to note that in this current work, the sample held at constant strain when tensile deformation was stopped. EBSD measurements for each step ($\varepsilon = 10\%$, 12% and 14%) started only after the stress relaxed and reached a constant value (after approximately 5 min).

2.3　EBSD analysis

Electron back-scattered diffraction (EBSD) technology was used for phase identification and orientation relationship (OR) analysis with the help of Nordlys S camera (Oxford instruments). After each interruption during the tensile work, one EBSD scan was performed for the welding zone. The data were input into TSL © software and HKL-Channel 5 © software for post-processing.

3　Results

Fig. 2 shows microstructure from the welding area before the *in-situ* SEM work. This area can be clearly divided into 3 zones which were marked by yellow and red dashed lines, respectively. Fusion zone, which locates at the left side of the image, occupied nearly 80% part of the welding zone. Within this zone, nearly all the laths exhibit acicular morphology. According to Migliarini's work[17] and Cyril's work[18], $\beta \rightarrow \alpha'$ transformation occurs during the welding processing, since the existence of high cooling gradient in welding zone. Therefore, we can deduce that these needle-like morphologies are α' laths. The fusion zone and 1st HAZ was separated by the yellow dashed line. Within 1st HAZ, this acicular morphology starts to globalize; and in the region of 2nd HAZ, globular shaped grains can be observed obviously. Hence, it can be clearly realized that this transition is from α' martensitic lath to α globular grains.

Before deformation, one EBSD map for the central part of fusion zone was obtained, it is shown in Fig. 3. The indexation level of this map was 62% and the step was 0.106 μm. In Fig. 3, full martensitic laths can be absolutely observed because of high cooling rate. Also it is worth to notice that for the following tensile work, the deformation direction was parallel to the positive direction of X axis (horizontal direction).

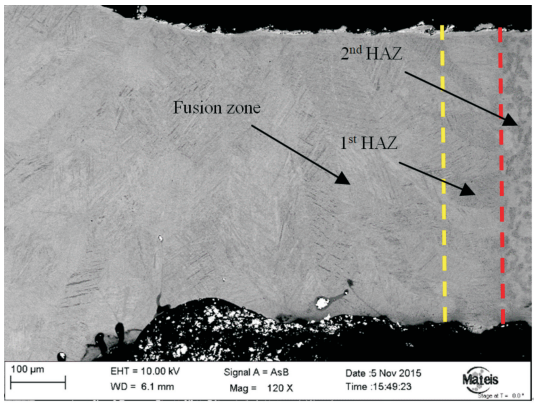

Fig. 2　SEM image for the welding area

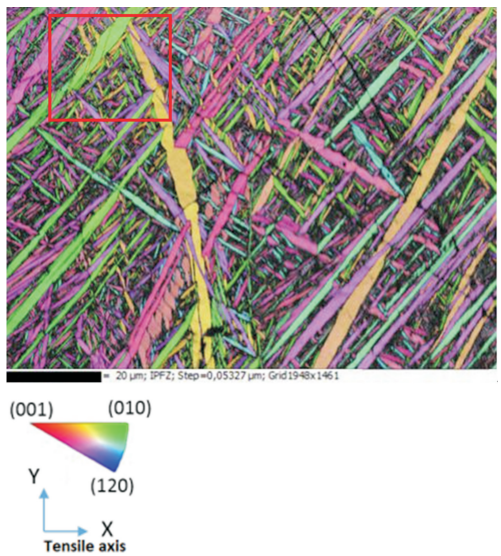

Fig. 3　An EBSD map for the central part of fusion zone before tensile test

During the tensile deformation, loading were interrupted twicly based on the microstructure evolution. The strain of the deformation was 10.8% and 12.3% respectively when the deformation was stopped. The engineering stress-strain curve was presented in Fig. 4. It can be seen clearly that the deformation was stopped firstly ($\varepsilon = 10.8\%$) as soon as the material has just yielded, which can be considered as the starting line of plastic deformation. The whole test ended at 14.2% deformation, although the sample was not ruptured in order to avoid the influence of severe plastic deformation on EBSD mapping.

EBSD scanning were carried out on the same area of which was shown in Fig. 3, while the strain were 10.8%,

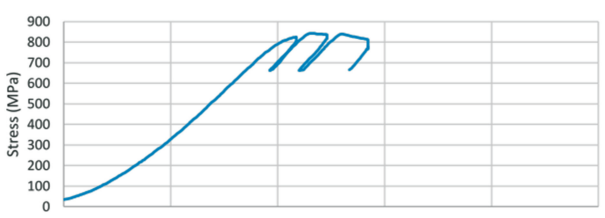

Fig. 4　Engineering stress-strain curve for this welding sample

12.3% and 14.2%, respectively, correlating to the two interruptions and ending point from the stress-strain curve.

As shown in Fig. 5, it is seen that due to the plastic deformation, both of lath morphology distorts and the new crystallography orientations can be observed, which were indicated by red arrows.

It is needed to mention that the EBSD data for the first interruption, $\varepsilon = 10.8\%$, was not taken into consideration in the following parts of this current work, because no obvious variations in crystallographic orientation can be found. This may be associated with the fact that plastic deformation has just started at $\varepsilon = 10.8\%$, which may result in less slip system or less twinning system being activated.

4 Discussion

The development of this section was based on the EBSD results of the *in-situ* tensile test of the welded Ti-6Al-4V sample. Full martensitic α' laths can be observed in this mapping zone. EBSD maps, which were gained before and after deformation, are shown in Fig. 5.

Before analyzing microstructure evolution, 3 particular laths were selected and marked as A, B and C, respectively (see in Fig 5). These 3 laths exhibit different orientations, which can be easier to analyze the variation of morphology and orientation before and after the deformation.

It can be observed that the coarse laths seem to deform seriously when comparing to the fine laths. For instance, lath B was sliced during deformation; meanwhile the lath A and C rotated to novel orientation instead of being sliced. This rotation is associated with accommodation of the deformation and can verify the existence of slipping.

Before deformation, lath A presents a <010> direction parallel to the tensile direction, while after deformation it tends to align the <120> direction parallel to the tensile direction. This phenomenon can be observed on all the laths with the same<010> direction.

As it is well-known, slipping and twinning are the two paths for deformation. It is necessary to analyze the deforming ways during the tensile test. The localization of the deformation was determined firstly; then these two deformation paths were discussed respectively.

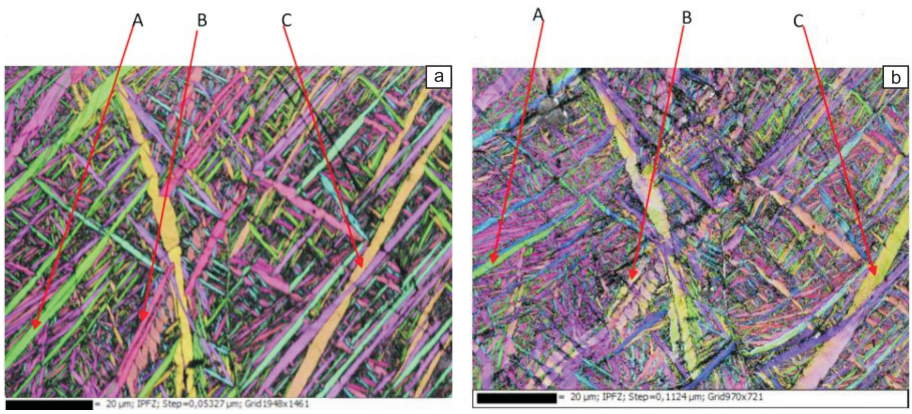

Fig. 5 EBSD maps for specimens before deformation (a) and when $\varepsilon = 14.2\%$ (b)

4.1 Localization of the plastic deformation

Combining Cyril's work[18] of local Green-Lagrange deformation tensors calculation and the morphology of the laths from Fig. 5 together, it can be indicated that the coarse laths-have undertaken higher strains than fine laths during the deformation processing. Moreover, highest strain means highest shear stress. Hence, it is reasonable to consider that both slipping systems and twinning systems are more likely to be activated in coarse laths. This may explain the reason why gradient of crystallographic orientation (i.e. a color gradient on the map) exists within the laths after deformation.

4.2 Analysis of slip: rotation of the grains

If focusing on the selected zone which was marked by red rectangle in Fig. 3, it can be clearly verified that slip bands exist within the coarse laths (as shown in Fig. 6), which means that slipping is the main plastic mechanism for coarse laths.

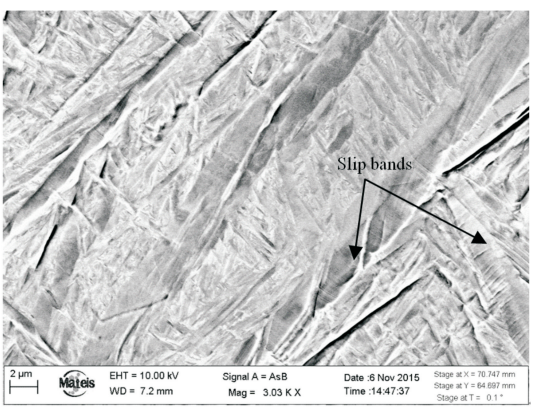

Fig. 6 SEM image for the selected zone from Fig. 3 at $\varepsilon = 14.2\%$

Thanks to the EBSD map, variation of crystallographic orientation for the laths can be extracted and analyzed individually. The first set of orientation identification is given in Fig. 7. This lath, which was extracted from the region marked by red rectangle in Fig. 3, was initially oriented <010>//TA (tensile axis) and rotated to align the direction <120> with the tensile axis due to deformation.

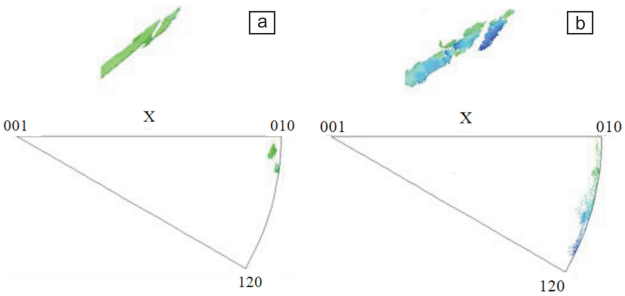

Fig. 7　Inverse Pole Figures(IPF-X) for the extracted lath from the selecting zone at initial state (a) and $\varepsilon = 14.2\%$ (b)

If only focusing on the laths with the orientation <010>// TA, after deformation, all the laths follow the same rotation path, from <010> to <120>//TA. This mode of deformation is also observed in globular microstructure of the heat affected zone, which was shown in Fig. 8 (2^{nd} HAZ). As shown in Fig. 8, some globular grains exhibit nearly the same color gradient as the laths discussed previously, which means, during the deformation, the globular grains with <010> // TA orientation are engaged in the same rotation as the martensitic lath with <010> // TA orientation.

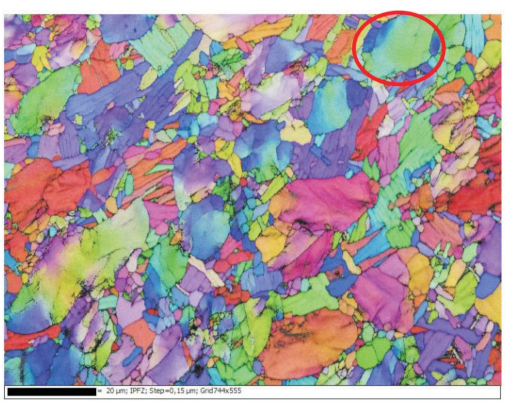

Fig. 8　EBSD map for 2^{nd} HAZ at $\varepsilon = 14.2\%$

By isolating one of grains from Fig. 8 (the grain encircled by red line) and plotting the related inverse pole figure (see in Fig. 9), it can be clearly seen that the crystallographic orientations vary in the same way. The green color links to a <010>//TA orientation and the dark blue color links to a <120>//TA orientation. Although this map only presented the orientation information in $\varepsilon = 14.2\%$ deformation stage, based on the result for the martensite microstructure (see Fig. 7), it is reasonable to deduced that in the initial stage, the considered grain was also oriented <010>//TA.

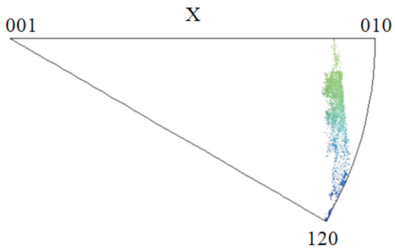

Fig. 9　IPF-X for the red circled grain in Fig. 8

According to those two independent observations, which were managed on one pure α' lath microstructure and globular grain, it is sound to deduced that this deformation mode may be followed in the non-welding zone which has globular morphology.

Therefore, it can be concluded that slipping exists in this Ti-6Al-4V alloy within the deformation procedure. Grains tend to align the direction <120> with the tensile axis by the method of rotation. Such rotation is facilitated if the grains have an initial orientation <010>//TA.

4.3　Analysis of twining

Apart from slipping, twining is another deformation way during the deformation procedure for hexagonal titanium cell. Lath B, which is arrowed in Fig. 5, shows the variation of orientation for different deformation steps(see in Fig. 10).

In Fig. 10a ~ 10c, orientation of lath B were shown for initial state, $\varepsilon = 12.3\%$, $\varepsilon = 14.6\%$ respectively. Based on the calculating result from CaRine software©, lath B has the initial orientation of $<\bar{1}24>$//TA. It is worth to note that this orientation is not close to <010>//TA.

When the loading was stopped at $\varepsilon = 12.3\%$, two parts of lath B (circled in red) present a new orientation <010>// TA, which are shown in Fig. 10b and also indicated by red circle. However, the rest part of lath B still keeps initial orientation ($<\bar{1}24>$//TA) with only small rotation.

Except for the slipping behavior which was discussed before, no obvious crystallographic orientation gradient can be related to the appearance of new orientation in the IPF(see in Fig. 10b). This may result from initial orientation of lath B is not close to <010>//TA, slipping system cannot be activated directly within this deforming period($\varepsilon < 12.3\%$).

This truth that some parts of the lath exhibit novel orientation without any obvious orientation gradient can be able to testify the existence of twinning behavior during plastic deformation. Linking the tensile twining relationship to EBSD data, it can be conveniently acquired that $\{122\}\langle\overline{1}21\rangle$ twinning system exists here.

Comparing Fig. 10b with Fig. 10c, it is interesting to find that no fresh crystallographic orientation can be observed within the un-twined part of lath B during the further deformation (ε = 12.3% ~ 14.2%). This gives the evidence that the lath B is no longer activated for twinning in further deformation.

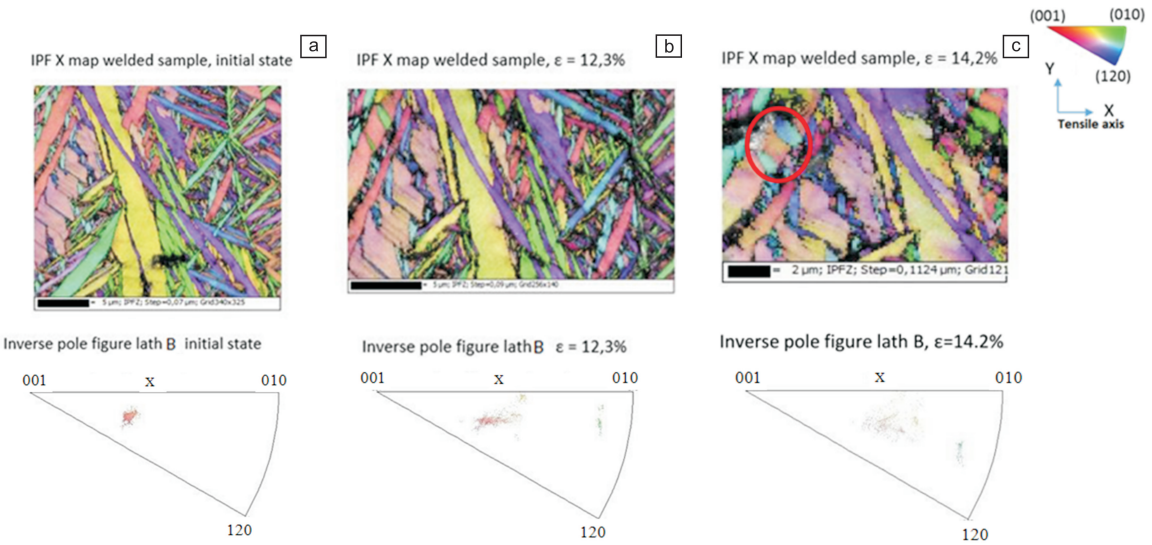

Fig. 10 Comparison of EBSD map and IPF-X for lath B at initial state (a), ε = 12.3% (b) and ε = 14.2% (c)

It is worth to notice that, according to the map from Fig. 10c, crystallographic orientation gradient can be observed clearly. It can be inferred that for this further deformation (from ε = 12.3% to ε = 14.2%), the whole lath rotate and two different slipping systems are activated for these twin and un-twined parts.

Furthermore, the twinning parts of the lath shows the orientation close to <120>//TA, which means in further deformation, from ε = 12.3% to ε = 14.2%, this twinning parts may rotate as the same way as the laths discussed before, from <010>//TA to <120>//TA

Therefore, in this case, it can be considered that twinning behavior may appear in lath B where the rotation by slipping is hindered due to the initial $\langle\overline{1}24\rangle$//TA orientation. With the help of this twinning behavior, new orientation, which is close to <010>//TA, can be able to rotate toward <120>//TA with less handicaps in further deformation. This rotation is accompanied by the appearance of orientation gradient which can testify the existence of slipping in this part. Simultaneously, the un-twinning part in lath B can be activated for slipping deformation instead of twinning deformation in the following deformation procedure.

5 Conclusions

Based on the results from *in-situ* tensile test with SEM and EBSD mapping, a systematic analysis of the plastic behavior in the laser welding Ti-6Al-4V alloy has been conducted. By comparing the orientations and morphologies of the laths, several conclusions can be obtained.

(1) Martensitictrans formation $\beta \rightarrow \alpha'$ occurs at the welding zone during the laser welding process, due to the high welding temperature and high cooling rate;

(2) Within the fusion zone, only acicular morphology exists. Meanwhile, in the 1st and 2nd HAZ, the morphology globalizes gradually. Especially, in 2nd HAZ, only globular morphology can be observed. Generally speaking, distinguished microstructural gradient exists in this Ti-6Al-4V alloy welding joint;

(3) During the tensile deformation processing, the grains within the welding zone tend to align crystallographic orientation <120>//TA (tensile axis) by rotating themselves. Within the first stage of this procedure, either slipping or twinning may occur, and this depends on the initial crystallographic orientation of the grains in the deforming zone. If the initial orientation can respect this alignment by rotation, such as close<010>//TA (tensile axis), only slipping exists in the deformation; If rotation cannot make the initial orientation respect the alignment directly, such as$\langle\overline{1}24\rangle$//TA for the initial orientation, twinning behavior may occur at parts of the

deformed grain firstly in order to modify this initial crystallographic orientation. Then the plastic deformation can be put forward by rotating and slipping.

References

[1] Lutjering G, Williams J C. *Titanium. 2nd Edition* [M]. Heidelberg: Springer, 2007.

[2] Rack H J, Qazi J I. *Materials Science and Engineering*[J], 2006, C26: 1269-1277.

[3] Boyer R R. *Materials Science and Engineering A*[J], 1996, 213: 103-114.

[4] BalasubramanianM, Jayabalan V, Balasubramanian V. *Materials Letters*[J], 2008, 62(6-7): 1102-1106.

[5] Blackburn J E, Allen C M, Hilton P A, *et al*. *Science and Technology of Welding and Join*[J], 2010, 15(5): 433-439.

[6] Li C, Muneharua K, Takao S, *et al*. *Materials and Design*[J], 2009, 30(1): 109-114.

[7] Saresh N, Pillai M G, Mathew J. *Journal of Materials Processing Technology*[J], 2007, 192-193(1): 83-88.

[8] Zhang Y, Sato Y S, Kokawa H, *et al*. *Materials Science and Engineering A*[J], 2008, 485(1): 448-455.

[9] Akman E, Demir A, Camel T, *et al*. *Journal of Materials Processing Technology*[J], 2009, 209 (8): 3705-3713.

[10] Liu J, Watanabe I, Yoshida K, *et al*. *Dental Materials*[J], 2002, 18(2): 143-148.

[11] Qi Y L, Deng J, Hong Q, *et al*. *Materials Science and Engineering A*[J], 2000, 280(1): 177-181.

[12] Zhang J X, Xue Y, Gong S L. *Science and Technology of Welding and Joining*[J], 2005, 10(6): 643-646.

[13] Gao X L, Zhang L J, Liu J, *et al*. *Materials Science and Engineering A*[J], 2013, 559(1): 14-21.

[14] Cao X J, Jahazi M. *Optics and Lasers in Engineering*[J], 2009, 47(11): 1231-1241.

[15] Squillace A, Prisco U, Ciliberto S, *et al*. *Journal of Materials Processing Technology*[J], 2012, 212(2): 427-436.

[16] Zhang J X, Song X, Zheng L. *Engineering Fracture Mechanics* [J], 2012, 83: 1-7.

[17] Migliarini A. *Thesis for Doctorate*[D]. Villeurbanne, France: INSA-Lyon, 2014.

[18] Cyril L. *Thesis for Master* [D]. Villeurbanne, France: INSA-Lyon, 2016.

（编辑　惠　琼）